*Electronic Supplementary Information (ESI) for*

# Mechanochemical Synthesis of 0D and 3D Cesium Lead Mixed Halide Perovskites

Abhoy Karmakar, Mya S. Dodd, Xiaoyue Zhang, Meagan S. Oakley, Mariusz Klobukowski and Vladimir K. Michaelis*

*Department of Chemistry, University of Alberta, Edmonton, Alberta, T6G 2G2, Canada*

**Corresponding author: vladimir.michaelis@ualberta.ca*

# Table of Contents

## Experimental

## Materials and Methods

All starting precursor materials were obtained from commercial sources and used without further purification: lead (II) iodide (99%), lead (II) bromide (+98%) and lead (II) chloride (99%) from ACROS Organics (Morris Plains, NJ, USA); CsBr, CsCl, and CsBr from Sigma Aldrich.

*Mechanochemical Synthesis of 3D $CsPbX_3X'_{3-x}$ (X and X' = Cl, Br, I and x = 0 to 3):*

Mechanochemical synthesis (MCS) has become a popular solvent-free method to obtain inorganic and organic-inorganic metal halide perovskite materials.[1–8] Using an similar approach 3D LHP parent compounds and their respective MHPs were prepared by the MCS route via manual hand grinding (HG) using a mortar and pestle for 2 hours under ambient conditions. To achieve the desired composition of the final product, the appropriate molar ratio of the starting material was loaded. For example, to synthesize (i) the parent compounds, $CsPbX_3$ (X = Cl, Br and I), 1:1 molar ratios of CsX and $PbX_2$ were used as the starting materials, (ii) MHPs like $CsPbCl_{1.5}Br_{1.5}$, equimolar amounts of CsCl, CsBr, $PbCl_2$ and $PbBr_2$ were used. The phase purity of the MCS products were examined using powder XRD after the synthesis. For $CsPbX_3$ (X = Cl and Br) and Cl/Br MHPs ($CsPbCl_3Br_{3-x}$), desired perovskite phases were obtained by the MCS-HG process (confirmed by powder X-ray diffraction (XRD)). For $CsPbI_3$ and Br/I MHPs ($CsPbBr_3I_{3-x}$), yellowish coloured non-perovskite phases were obtained by MCS-HG and thus they were further treated by thermal annealing (220-350 °C) under ambient conditions.

*Mechanochemical Synthesis of 0D $Cs_4PbX_xX'_{6-x}$ (X and X' = Cl, Br and x = 0 to 6):*

Zero dimensional $Cs_4PbX_6$ (X = Cl, Br) parent and $Cs_4PbCl_3Br_3$ MHP compounds were prepared by the MCS route via manual hand grinding using a mortar and pestle for 2 hours under ambient conditions. To achieve the desired composition of the final product, the appropriate molar ratio of the starting material was loaded. For example, to synthesize (i) the parent compounds, $Cs_4PbX_6$ (X = Cl, Br), 4:1 molar ratios of CsX and $PbX_2$ were used as the starting materials, (ii) $Cs_4PbCl_3Br_3$ MHP, CsCl, CsBr,

$PbCl_2$ and $PbBr_2$ were used with a molar ratio of 4:4:1:1. The phase purity of the MCS products were examined using XRD after the synthesis. Unfortunately, obtaining a phase-pure $Cs_4PbI_6$ material using the same approach was unsuccessful.

Worth noting are two minor impurity phases that appear during the MCS of 0D LHPs. We can clearly identify one as the starting material (CsX, *ca.* 1%), while the other is an unidentified Cs-containing phase (*ca.* 5%) as shown in Fig. 1f and S7. We further note these two impurities remain unaltered upon further hand grinding (i.e. up to 1 hour). MCS is a suitable synthesis approach to avoid other stable ternary cesium lead halide compounds such as 3D $CsPbX_3$ and 2D $CsPb_2X_5$ impurities as indicated by $^{133}Cs$ NMR analysis (Fig S7).

*Powder X-ray Diffraction (XRD):*

The XRD measurements were obtained under ambient laboratory conditions on an Inel MPD multi-purpose diffractometer (40 kV, 50 mA) system (Department of Chemistry, University of Alberta) equipped with a CPS 120 curved position sensitive X-ray detector and Cu $K_\alpha$ radiation source (1.540596 Å). All the samples were placed on a plastic sample holder and 2θ scans between $0^o$ to $114^o$ with a step increment of $0.029^o$ were obtained.

*Diffuse Reflectance (DR) Spectroscopy:*

The DR spectra of the samples were collected on a Cary 5000 UV/Vis/NIR spectrophotometer (Analytical and Instrumental Laboratory, Department of Chemistry, University of Alberta), equipped for the analysis of small-quantity fine powdered samples. Each sample (~ 50 to 100 mg) was packed into a black boat and measurement was acquired between 200 and 1000 nm wavelength with a 100 % reflectance standard.

The DR spectra were converted to pseudo-absorbance spectra using the following Kubelka-Munk transformation:[9] $\alpha \sim (1\text{-}R)^2/(2R)$, where, R and α are the absolute reflectance and pseudo-absorbance, respectively. The direct bandgaps are obtained by taking the intercept upon extrapolation of the linear regions of $(\alpha h\nu)^2$ vs E(eV) plot.

Solid-State Nuclear Magnetic Resonance (NMR) Spectroscopy:

*Lead-207 NMR:* $^{207}$Pb NMR data were acquired under non-spinning conditions for samples packed in 4 mm OD $ZrO_2$ rotors at 11.75 and 21.14 T, on a Bruker Avance 500 and Avance II 900 NMR spectrometers, respectively. All $^{207}$Pb NMR data were collected using a 4 mm double resonance H/X Bruker probe, using a Hahn-echo pulse sequence[10] i.e., $(\pi/2)_x - \tau_1 - (\pi)_y - \tau_2 -$ ACQ, where $\tau_1$ and $\tau_2$ are the inter-pulse and refocusing delays, respectively, or a modified quadrupolar-echo pulse sequence to achieve broader excitation width and minimize line distortions at higher magnetic field strengths. A recycle delay of 4 - 20 s was used for the samples. For the MHP samples, a variable offset cumulative spectra (VOCS)[11] approach was used with between three and five steps and a 30 kHz (for 11.75 T) or 50 kHz (for 21.14 T) transmitter stepping frequency across the spectral range to get a complete and undistorted spectrum; the sub-spectra were added using the skyline projection method. Two-dimensional $^{207}$Pb-$^{207}$Pb exchange spectroscopy (EXSY)[12] NMR spectra were acquired at 21.14 T by using mixing times between 50 μs and 50 ms. A total of 24-128 slices were collected in the indirect dimension using a 2 μs increment, and between 128 and 1,024 transients were acquired per slice. All $^{207}$Pb NMR spectra were referenced to $PbMe_4$ ($\delta(^{207}Pb) = 0.00$ ppm) by setting $\delta(^{207}Pb) = -647.5$ ppm for solid $MAPbCl_3$ at 293 K.[13]

*Caesium-133 NMR:* $^{133}$Cs NMR data were acquired at 11.75 T on a Bruker Avance 500 spectrometer under magic-angle spinning (MAS) conditions using a spinning frequency of 13 kHz. All samples were packed into 4 mm OD $ZrO_2$ and a Bloch pulse sequence was used with a 1.25 μs pulse width (~20° tip angle), 1–16 co-added transients and 120 s recycle delay.

NMR Data Processing and Analysis: NMR spectra were processed using Topspin 3.5 Bruker software with between 25 and 500 Hz exponential apodization and plotted using OriginPro 8 software. The $^{207}$Pb

NMR peak maxima ($\delta_{cs}$($^{207}$Pb)) are reported for the CsPbX$_3$ (X = Cl, Br, I) parent perovskite phases due to the broad lineshapes. The $^{207}$Pb NMR chemical shift anisotropy for δ-CsPbI$_3$ was simulated using the WSOLIDS software[14].

*Quantum Chemical Calculations:* Cluster models of the octahedral lead halide, $[PbX_{6-x}X'_x]^{4-}$, were used to calculate the theoretical $^{207}$Pb NMR shielding and tensor values. Average bond lengths were taken from the appropriate dimension crystal structure, where 3D geometries gave r(Pb-Cl) = 2.843 Å, r(Pb-Br) = 2.966 Å, and r(Pb-I) = 3.146 Å, and the 0D structures gave r(Pb-Cl) = 2.513 Å, and r(Pb-Br) = 3.028 Å.[15–18] Density functional theory, specifically the generalized gradient approximation functional PBE,[19] was used within the Amsterdam Density Functional (ADF) program (Version 2016-07-01).[20–22] The zero order regular approximation[23] (ZORA) with the appropriate Slater-type all-electron triple-zeta polarized (ZORA/TZP) basis set was used to describe scalar relativistic effects and spin-orbit coupling present within the heavy-metal cluster. The calculations were performed without symmetry in order to generate $^{207}$Pb NMR shielding and tensors incorporating relativistic effects. In order to compare calculated and experimental chemical shifts, the theoretical shielding constants were converted to chemical shifts using $\delta_{calc}(ppm) = -(\sigma_{calc} - 8583\ ppm)$ for both the 3D and 0D materials. This relationship was determined from a linear regression between experimental chemical shifts and the calculated magnetic shielding values of the parent compounds for both 3D and 0D materials.

**Table S1. $^{207}$Pb and $^{133}$Cs NMR parameters for 3D CsPbX$_3$ (X = Cl, Br, I) and 0D Cs$_4$PbX$_6$ (X = Cl, Br) parent perovskites ($B_0$ = 11.75 T).**

| Samples | $^{207}$Pb non-spinning NMR | | $^{133}$Cs MAS NMR | |
|---|---|---|---|---|
| | $^{a}\delta_{cs}$($^{207}$Pb)/ppm | fwhm/kHz | $\delta_{cs}$($^{133}$Cs)/ppm | fwhm/Hz |
| CsPbCl$_3$ | −728 (1) | ~ 5 | 76.9 (0.1) | 155 (5) |
| CsPbBr$_3$ | 244 (5) | ~ 18 | 110.3 (0.2) | 238 (5) |
| Black γ-CsPbI$_3$ | 1265 (20) | ~ 25 | 166.9 (0.3) | 390 (10) |
| Yellow δ-CsPbI$_3$ | 1065 (15)$^{b}$ | -$^{c}$ | 247.0 (0.2) | 385 (5) |
| Cs$_4$PbCl$_6$ | −1139 (1) | ~ 4.5 | 185.0 (0.1) | 165 (5) |
| Cs$_4$PbBr$_6$ | −385 (5) | ~ 14 | 224.9 (0.1) | 305 (5) |

$^{a}$Chemical shift at peak maxima, $\delta_{cs;}$ $^{b}$ Isotropic chemical shift, $\delta_{iso}$; $^{c}$ Span (Ω) = 650 (30) ppm, skew (κ) = 0.7 (0.1)

**Table S2. $^{207}$Pb magnetic shielding parameters from octahedral $[PbX_{6-x}X'_x]^{4-}$ anionic clusters from DFT calculations. $\sigma_{iso}$ = isotropic shielding constant, $\Omega$ = span, and $\kappa$ = skew.**

(a) 3D Materials:

| Environments | $\sigma_{iso}$ (ppm) | $\Omega$ (ppm) | $\kappa$ |
|---|---|---|---|
| $[PbCl_6]^{4-}$ | 9381.77 | 0.0 | 0 |
| $[PbCl_5Br]^{4-}$ | 9239.67 | 10.3 | 0.99 |
| cis-$[PbCl_4Br_2]^{4-}$ | 9098.6 | 9.8 | 0.13 |
| trans-$[PbCl_4Br_2]^{4-}$ | 9102.63 | 15.7 | 0.99 |
| fac-$[PbCl_3Br_3]^{4-}$ | 8959.46 | 3.9 | -0.99 |
| mer-$[PbCl_3Br_3]^{4-}$ | 8962.06 | 24.6 | 0.67 |
| cis-$[PbCl_2Br_4]^{4-}$ | 8824.46 | 14.5 | -0.87 |
| trans-$[PbCl_2Br_4]^{4-}$ | 8825.71 | 54.9 | 0.99 |
| $[PbClBr_5]^{4-}$ | 8690.85 | 31.3 | 0.99 |
| $[PbBr_6]^{4-}$ | 8560.13 | 0.0 | 0.75 |
| $[PbBr_5I]^{4-}$ | 8394.72 | 81.4 | -1.00 |
| cis-$[PbBr_4I_2]^{4-}$ | 8243.18 | 109.9 | 0.91 |
| trans-$[PbBr_4I_2]^{4-}$ | 8224.02 | 211.9 | -1.00 |
| fac-$[PbBr_3I_3]^{4-}$ | 8109.09 | 4.9 | 0.99 |
| mer-$[PbBr_3I_3]^{4-}$ | 8091.06 | 253.8 | 0.02 |
| cis-$[PbBr_2I_4]^{4-}$ | 7978.04 | 143.2 | -0.97 |
| trans-$[PbBr_2I_4]^{4-}$ | 7963 | 283.4 | 1.00 |
| $[PbBrI_5]^{4-}$ | 7873.11 | 152.0 | 0.99 |
| $[PbI_6]^{4-}$ | 7796.52 | 0.0 | 0.00 |

(b) 0D Materials:

| Environments | $\sigma_{iso}$ (ppm) | $\Omega$ (ppm) | $\kappa$ |
|---|---|---|---|
| $[PbCl_6]^{4-}$ | 9210.36 | 0.0 | -1.00 |
| $[PbCl_5Br]^{4-}$ | 8556.83 | 460.5 | 0.78 |
| cis-$[PbCl_4Br_2]^{4-}$ | 8738.37 | 392.3 | 0.74 |
| trans-$[PbCl_4Br_2]^{4-}$ | 8944.73 | 527.5 | 1.00 |
| fac-$[PbCl_3Br_3]^{4-}$ | 8569.72 | 644.4 | -1.00 |
| mer-$[PbCl_3Br_3]^{4-}$ | 8712.53 | 812.4 | -0.22 |
| cis-$[PbCl_2Br_4]^{4-}$ | 8528.2 | 787.6 | -0.47 |
| trans-$[PbCl_2Br_4]^{4-}$ | 8758.8 | 1559.2 | -1.00 |
| $[PbClBr_5]^{4-}$ | 8509.47 | 896.4 | -1.00 |
| $[PbBr_6]^{4-}$ | 8421.84 | 0.0 | 0.00 |

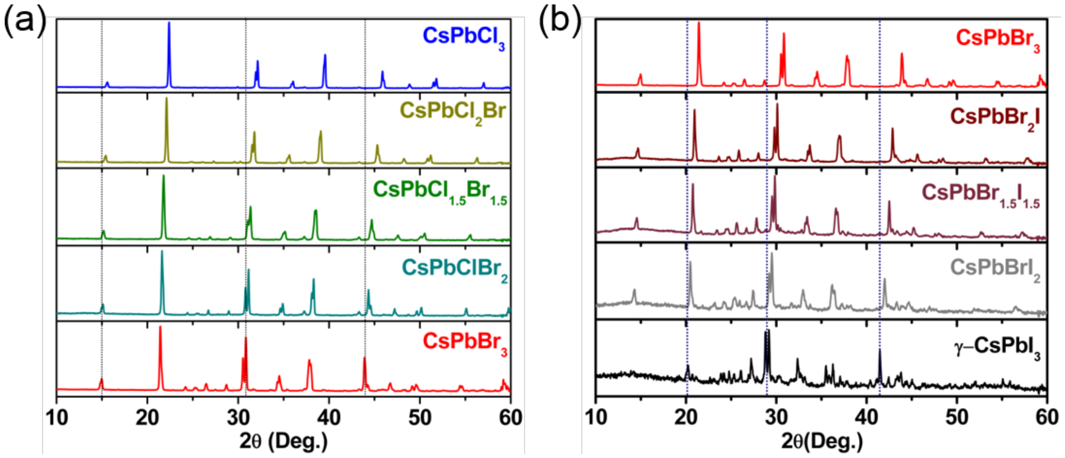

**Figure S1.** Room temperature powder XRD patterns for $CsPbCl_xBr_{3-x}$ (a), and $CsPbBr_xI_{3-x}$ (b), where $0 \leq x \leq 3$. The dotted lines are the guides to the eye.

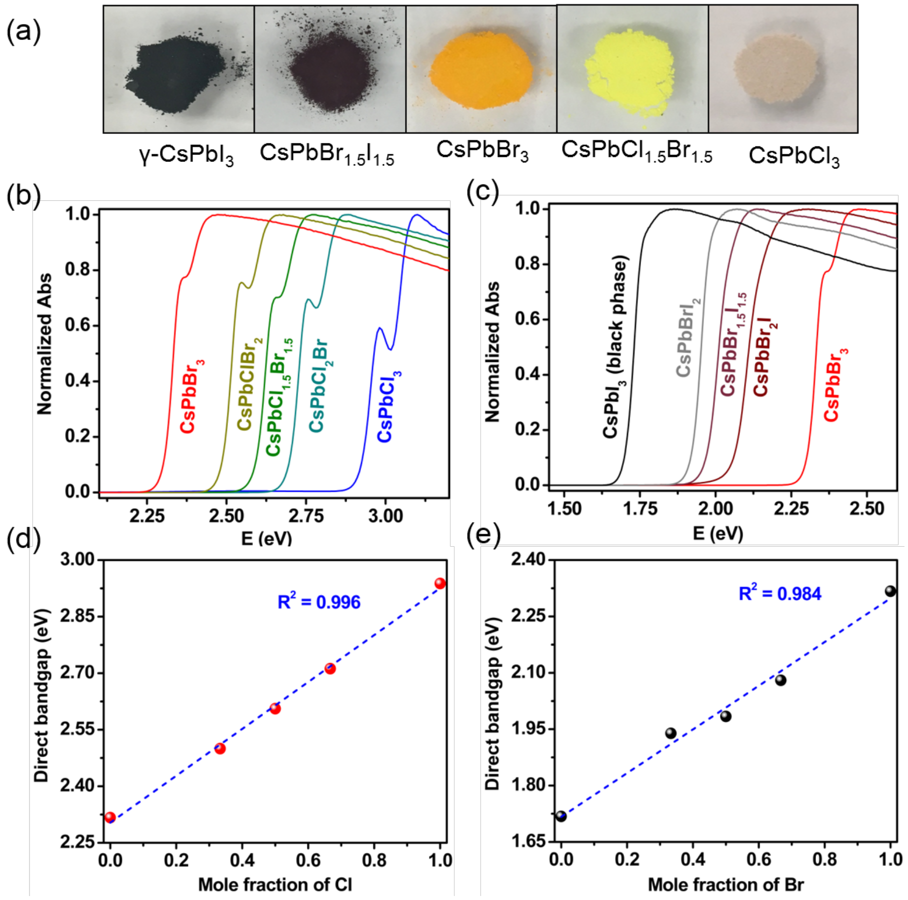

**Figure S2**. Photos of the 3D materials as indicated (a). Normalized absorbance spectra and direct bandgap relationship with halide composition for $CsPbCl_xBr_{3-x}$ (b and d, respectively) and $CsPbBr_xI_{3-x}$ (c and e, respectively), where $0 \leq x \leq 3$. The DR spectra were converted to absorbance by using the Kubelka−Munk equation and direct bandgaps are extracted from the Tauc plot (see Materials and Methods). The $CsPbCl_xBr_{3-x}$ materials were prepared only by MCS-HG, whereas for the $CsPbBr_xI_{3-x}$ materials, an additional thermal annealing step post-MCS was performed.

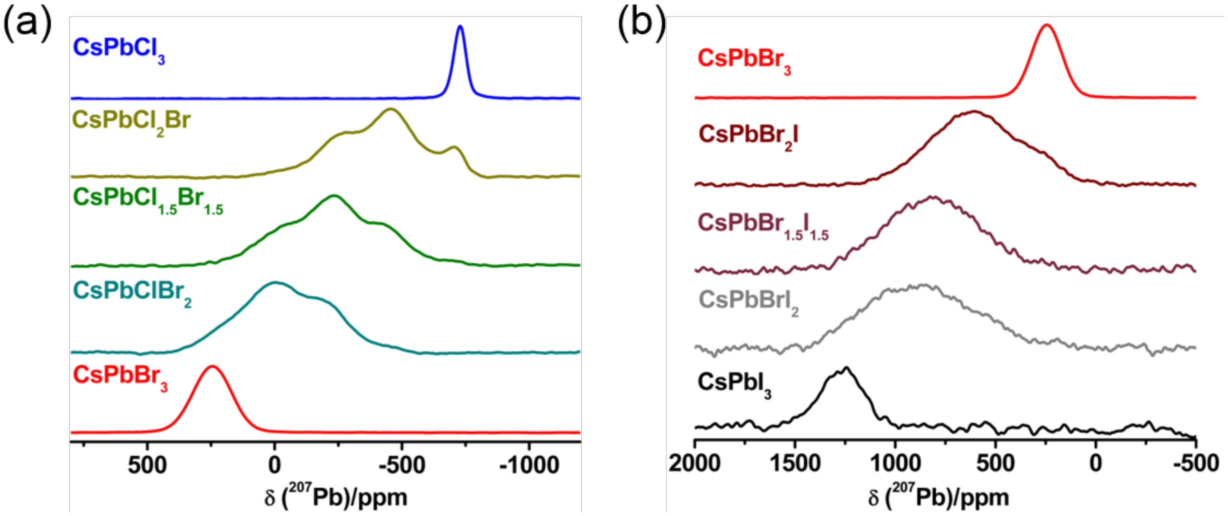

**Figure S3.** Room temperature $^{207}$Pb NMR spectra acquired at 11.75 T under non-spinning conditions for $CsPbCl_xBr_{3-x}$ (a), and $CsPbBr_xI_{3-x}$ (b), where $0 \leq x \leq 3$. The $CsPbCl_xBr_{3-x}$ materials were prepared only by MCS-HG, whereas an additional thermal annealing step post-MCS was performed for the $CsPbBr_xI_{3-x}$ materials.

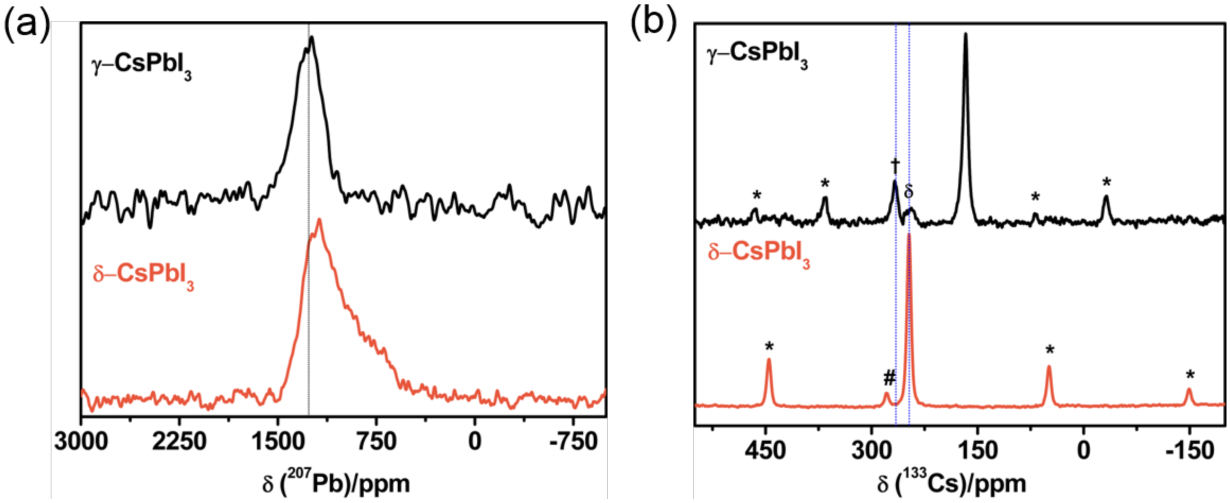

**Figure S4**. $^{207}$Pb (a) and $^{133}$Cs (b) NMR spectra for γ-$CsPbI_3$ (perovskite or black phase) and for δ-$CsPbI_3$ (non-perovskite or yellow phase), acquired at 11.75 T. The $^{207}$Pb NMR spectra were acquired under non-spinning sample conditions, whereas the $^{133}$Cs NMR spectra were acquired under MAS conditions at a spinning frequency of 13 kHz. The non-perovskite δ-$CsPbI_3$ phase was prepared by MCS and the corresponding perovskite phase γ-$CsPbI_3$ was obtained by thermal annealing at 350 °C. The dotted lines in (a) are guides to the eye showing that the $^{207}$Pb NMR chemical shift for γ-$CsPbI_3$ is higher in frequency compared to that for δ-$CsPbI_3$. The asterisks (∗), delta (δ), crosses (†), and hashtag (#) in (b) indicate spinning sidebands, δ-$CsPbI_3$, Cs-containing impurity and residual CsI, respectively.

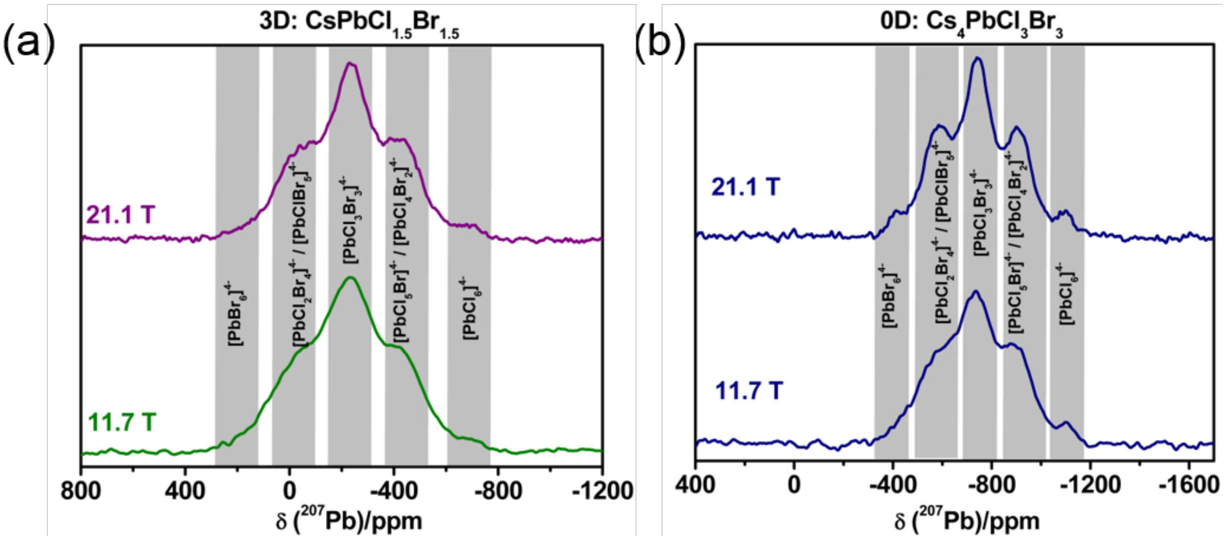

**Figure S5**. $^{207}$Pb NMR spectra for $CsPbCl_{1.5}Br_{1.5}$ MHP (a, 3D material) and $Cs_4PbCl_3Br_3$ MHP (b, 0D material) prepared by MCS, acquired at 11.75 and 21.1 T under non-spinning sample conditions. The unique $^{207}$Pb NMR chemical shifts of the corresponding DFT calculated $[PbCl_xBr_{6-x}]^{4-}$ octahedra (x = 0 to 6) are indicated by the highlighted regions within the spectra.

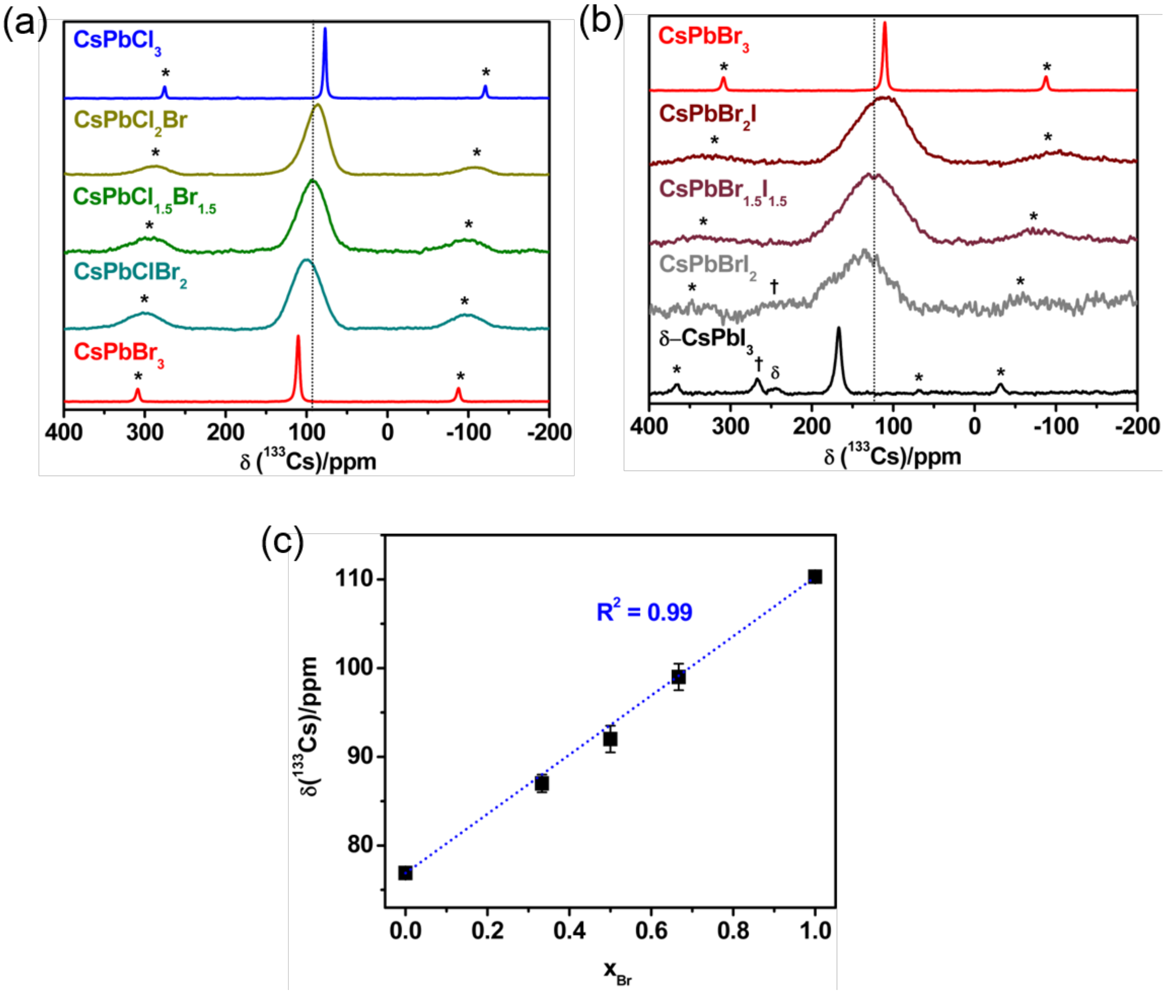

**Figure S6**. Room temperature $^{133}$Cs NMR spectra acquired at 11.75 T with an MAS frequency of 13 kHz for the $CsPbCl_xBr_{3-x}$ (a), and $CsPbBr_xI_{3-x}$ (b) series, where $0 \leq x \leq 3$. The linear fitting of $^{133}$Cs isotropic chemical shifts vs bromine mole-fraction for the $CsPbCl_xBr_{3-x}$ series is shown in (c). The $CsPbCl_xBr_{3-x}$ materials were prepared only by MCS-HG, whereas an additional thermal annealing step post-MCS was performed for the $CsPbBr_xI_{3-x}$ materials. The dotted lines in (a) and (b) are guides for the eye. The asterisks (*), dagger (†) and delta (δ) in (b) indicate spinning sidebands, Cs-containing impurity and δ-$CsPbI_3$, respectively.

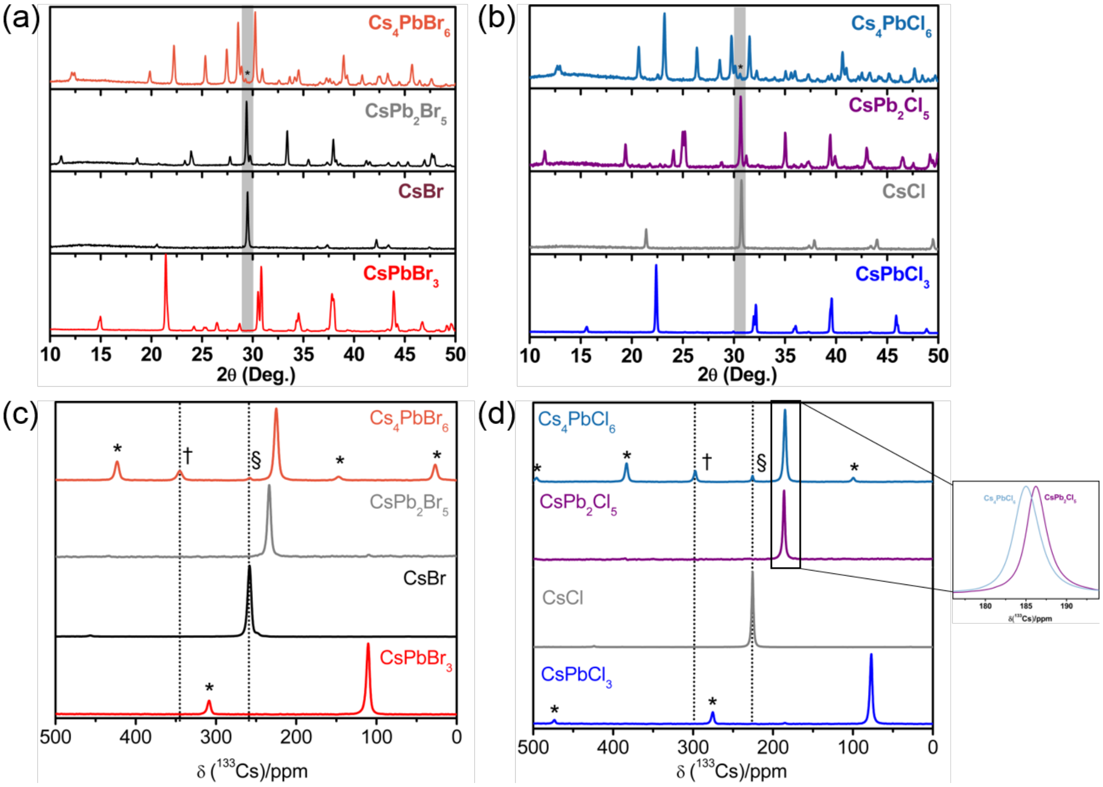

**Figure S7.** Room temperature powder XRD patterns (a and b) and $^{133}$Cs NMR (c and d) for 0D $Cs_4PbCl_6$ and $Cs_4PbBr_6$ materials, respectively. The XRD and $^{133}$Cs NMR are compared with their corresponding 2D $CsPb_2X_5$, 3D $CsPbX_3$ and CsX (X = Cl, Br). All the 0D, 2D and 3D materials were prepared by MCS-HG protocol. The asterisks (*) indicate the highly intense (110) peak of CsX, a starting material. The dotted lines are guides to the eye. Insert in (d) shows the slight but distinguishable $^{133}$Cs NMR chemical shift difference between 0D $Cs_4PbCl_6$ and 2D $CsPb_2Cl_5$ materials.

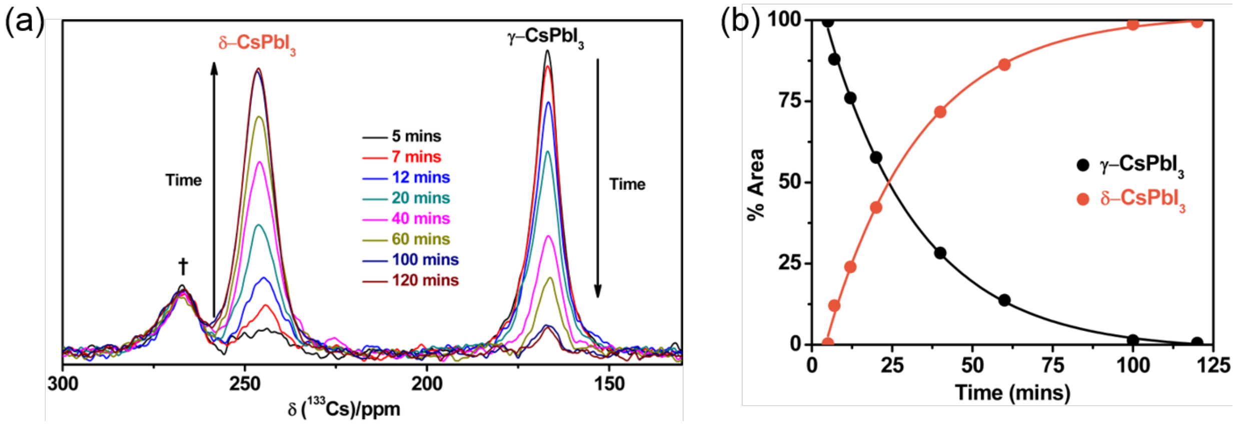

**Figure S8**. Room temperature $^{133}$Cs NMR spectra for CsPbI$_3$ (a) showing the perovskite, γ-CsPbI$_3$, to non-perovskite, δ-CsPbI$_3$, phase conversion over time. The freshly prepared γ-CsPbI$_3$ sample was packed in a 4 mm OD ZrO$_2$ rotor and the spectra were acquired at 11.75 T under magic-angle spinning at 13 kHz. Area (%) of $^{133}$Cs NMR spectra of γ- and δ-CsPbI$_3$ as a function of time (b). The fitting line suggests a first-order kinetics phase conversion mechanism with a half-life ($t_{1/2}$) of 29 ± 2 mins. The dagger (†) in (a) indicates Cs-containing impurity present within the sample.

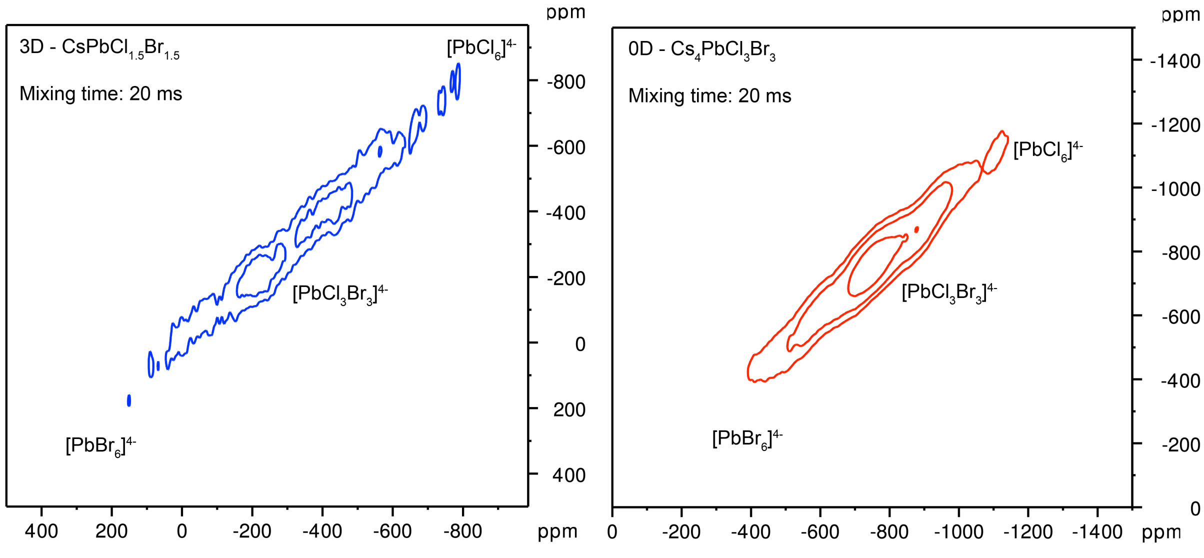

**Figure S9**. Room temperature non-spinning $^{207}$Pb-$^{207}$Pb EXSY NMR spectra for 3D CsPbCl$_{1.5}$Br$_{1.5}$ (left, blue) and 0D Cs$_4$PbCl$_3$Br$_3$ (right, red) MHP materials acquired at 21.14 T with a mixing time of 20 ms.

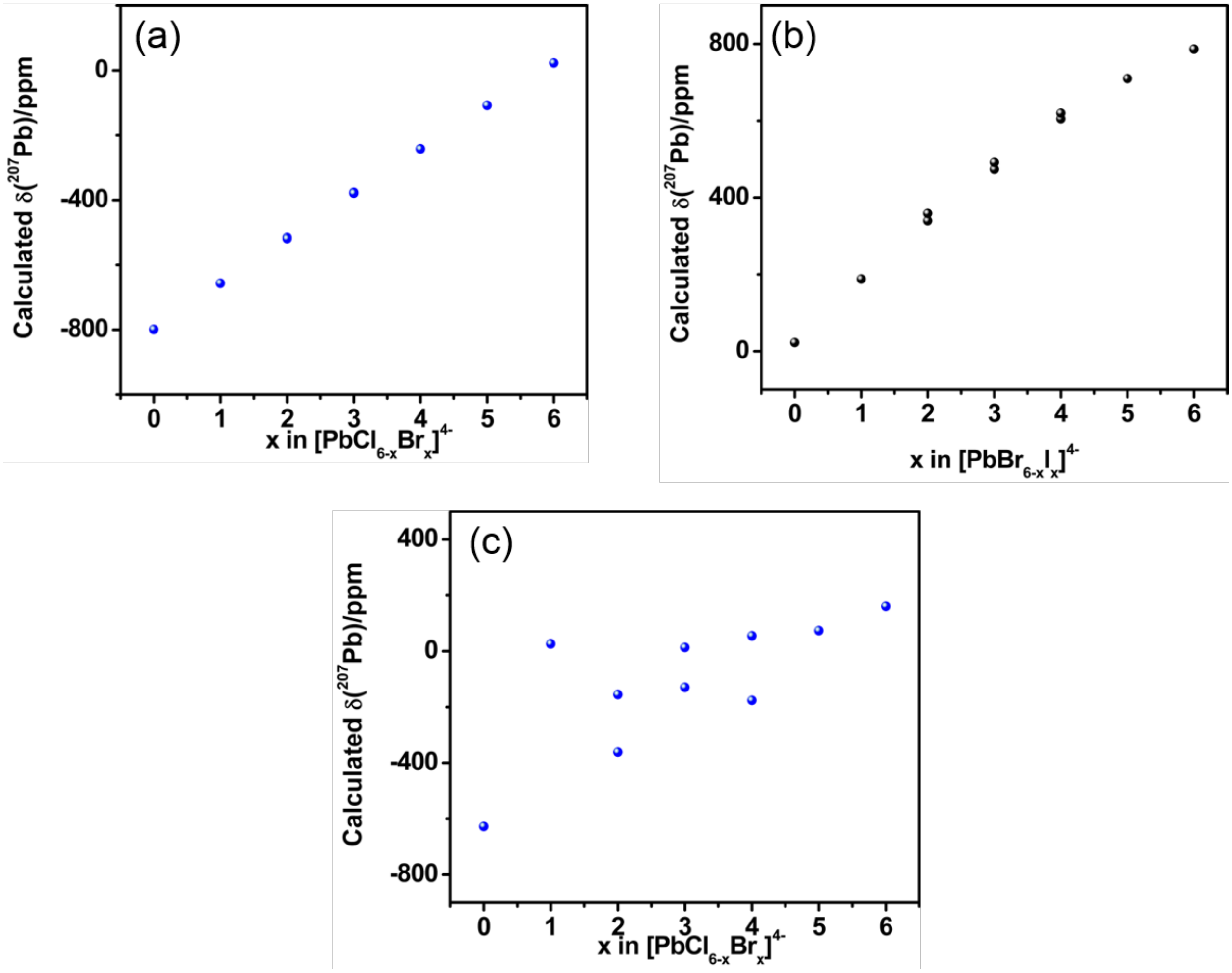

**Figure S10**. Calculated $^{207}$Pb NMR isotropic chemical shift with Br substitution in $[PbCl_{6-x}Br_x]^{4-}$ polyhedral (a, 3D materials), I substitution in $[PbBr_{6-x}I_x]^{4-}$ polyhedral (b, 3D materials), and Br substitution in $[PbCl_{6-x}Br_x]^{4-}$ polyhedral (c, 0D materials), where, x = 0 to 6.

# REFERENCES

1 J. Breternitz, S. Levcenko, H. Hempel, G. Gurieva, A. Franz, A. Hoser and S. Schorr, *arXiv*, 2018, (https://arxiv.org/ftp/arxiv/papers/1810/1810.1133.

2 S. Yun, A. Kirakosyan, S. Yoon and J. Choi, *ACS Sustain. Chem. Eng.*, 2018, **6**, 3733−3738.

3 M. Wilke and N. Casati, *Chem. - A Eur. J.*, 2018, **24**, 17701–17711.

4 O. Y. Posudievsky, N. V Konoshchuk, A. G. Shkavro, V. L. Karbivskiy, V. G. Koshechko and V. D. Pokhodenko, *ACS Appl. Nano Mater.*, 2018, **1**, 4145–4155.

5 D. J. Kubicki, D. Prochowicz, A. Hofstetter, S. M. Zakeeruddin, M. Grätzel and L. Emsley, *J. Am. Chem. Soc.*, 2018, **140**, 7232−7238.

6 D. Prochowicz, P. Yadav, M. Saliba, M. Saski, S. M. Zakeeruddin, J. Lewinski and M. Gratzel, *Sustain. Energy Fuels*, 2017, **1**, 689–693.

7 A. D. Jodlowski, A. Yépez, R. Luque, L. Camacho and de G. Miguel, *Angew. Chemie Int. Ed.*, 2016, **55**, 14972–14977.

8 Z. Zhu, Q. Yang, L. Gao, L. Zhang, A. Shi, C. Sun, Q. Wang and H. Zhang, *J. Phys. Chem. Lett.*, 2017, **8**, 1610–1614.

9 P. Kubelka and F. Munk, *Z.Tech. Phys. (Leipzig)*, 1931, **12**, 593–601.

10 E. L. Hahn, *Phys. Rev.*, 1950, **80**, 580–594.

11 D. Massiot, I. Farnan, N. Gautier, D. Trumeau, A. Trokiner and J. Pierre, *Solid State Nucl. Magn. Reson.*, 1995, **4**, 241–248.

12 J. Jeener, B. H. Meier, P. Bachmann and R. R. Ernst, *J. Chem. Phys.*, 1979, **71**, 4546–4553.

13 G. M. Bernard, A. Goyal, M. Miskolzie, R. McKay, Q. Wu, R. E. Wasylishen and V. K. Michaelis, *J. Magn. Reson.*, 2017, **283**, 14–21.

14 K. Eichele, *WSOLIDS NMR Simulation Package, 1.21.3; Universität Tübingen: Tübingen, Germany*, 2013.

15 M. Natarajan and B. Prakash, *Phys. Status Solidi A Appl. Res.*, 1971, **4**, K167–K172.

16 C. C. Stoumpos, C. D. Malliakas, J. A. Peters, Z. Liu, M. Sebastian, J. Im, T. C. Chasapis, A. C. Wibowo, D. Y. Chung, A. J. Freeman, B. W. Wessels and M. G. Kanatzidis, *Cryst. Growth Des.*, 2013, **13**, 2722−2727.

17 R. J. Sutton, M. R. Filip, A. A. Haghighirad, N. Sakai, B. Wenger, F. Giustino and H. J. Snaith, *ACS Energy Lett.*, 2018, **3**, 1787–1794.

18 M. De Bastiani, I. Dursun, Y. Zhang, B. A. Alshankiti, X. H. Miao, J. Yin, E. Yengel, E. Alarousu, B. Turedi, J. M. Almutlaq, M. I. Saidaminov, S. Mitra, I. Gereige, A. Alsaggaf, Y. Zhu, Y. Han, I. S. Roqan, J. L. Bredas, O. F. Mohammed and O. M. Bakr, *Chem. Mater.*, 2017, **29**, 7108–7113.

19 J. P. Perdew, K. Burke and M. Ernzerhof, *Phys. Rev. Lett.*, 1996, **77**, 3865–3868.

20 G. te Velde, F. M. Bickelhaupt, E. J. Baerends, C. Fonseca Guerra, S. J. A. van Gisbergen, J. G. Snijders and T. Ziegler, *J. Comput. Chem.*, 2001, **22**, 931–967.

21 C. F. Guerra, J. G. Snijders, G. te Velde and E. J. Baerends, *Theor. Chem. Acc.*, 1998, **99**, 391±403.

22 E. J. Baerends, T. Ziegler, A. J. Atkins, J. Autschbach, D. Bashford, O. Baseggio, A. Bérces, F. M. Bickelhaupt, C. Bo, P. M. Boerritger, L. Cavallo, C. Daul, D. P. Chong, D. V Chulhai, L. Deng, R. M. Dickson, J. M. Dieterich, D. E. Ellis, M. van Faassen, A. Ghysels, A. Giammona, S. J. A. van Gisbergen, A. Goez, A. W. Götz, S. Gusarov, F. E. Harris, P. van den Hoek, Z. Hu, C. R. Jacob, H. Jacobsen, L. Jensen, L. Joubert, J. W. Kaminski, G. van Kessel, C. König, F. Kootstra, A. Kovalenko, M. Krykunov, E. van Lenthe, D. A. McCormack, A. Michalak, M. Mitoraj, S. M. Morton, J. Neugebauer, V. P. Nicu, L. Noodleman, V. P. Osinga, S. Patchkovskii, M. Pavanello, C. A. Peeples, P. H. T. Philipsen, D. Post, C. C. Pye, H. Ramanantoanina, P. Ramos, W. Ravenek, J. I. Rodríguez, P. Ros, R. Rüger, P. R. T. Schipper, D. Schlüns, H. van Schoot, G. Schreckenbach, J. S. Seldenthuis, M. Seth, J. G. Snijders, M. Solà, S. M., M. Swart, D. Swerhone, G. te Velde, V. Tognetti, P. Vernooijs, L. Versluis, L. Visscher, O. Visser, F. Wang, T. A. Wesolowski, E. M. van Wezenbeek, G. Wiesenekker, S. K. Wolff, T. K. Woo and A. L. Yakovlev, *ADF2018, SCM, Theor. Chem. Vrije Univ. Amsterdam, Netherlands, http//www.scm.com*.

23 P. Philipsen, E. van Lenthe, J. Snijders and E. Baerends, *Phys. Rev. B*, 1997, **56**, 13556–13562.